DOI: 10.1002/ejic.200500682

Hybrid Inorganic–Organic 1D and 2D Frameworks with $[As_6V_{15}O_{42}]^{6-}$ Polyoxoanions as Building Blocks

Shou-Tian Zheng,[a] Yong-Mei Chen,[b] Jie Zhang,[a] Ji-Qing Xu,[c] and Guo-Yu Yang*[a,d]

Keywords: Polyoxometalate / Vanadium / Arsenic

Three novel heteropolyoxovanadates, $[Ni(2,2'\text{-bpy})_3]_2[\{Ni(en)_2\}As_6V_{15}O_{42}(H_2O)]\cdot 9.5H_2O$ (**1**), $[Zn_2(dien)_3(H_2O)_2]_{1/2}\{[Zn_2(dien)_3]As_6V_{15}O_{42}(H_2O)\}\cdot 2H_2O$ (**2**), and $[Co(enMe)_2]_3[As_6V_{15}O_{42}(H_2O)]\cdot 2H_2O$ (**3**), were hydrothermally synthesized and characterized by single-crystal X-ray diffraction. Crystal data: **1**, monoclinic, $P2_1/n$, a = 14.0324(9) Å, b = 13.9900(8) Å, c = 30.5785(19) Å, β = 102.861(1)°, Z = 2; **2**, monoclinic, $P2_1/c$, a = 13.361(5) Å, b = 23.979(8) Å, c = 22.873(8) Å, β = 102.459(4)°, Z = 4; **3**, triclinic, $P\bar{1}$, a = 13.2976(1) Å, b = 15.0583(1) Å, c = 20.1661(2) Å, α = 85.620(8)°, β = 79.553(9)°, γ = 65.087(9)°, Z = 2. Compound **1** consists of 1D $[\{Ni(en)_2\}As_6V_{15}O_{42}(H_2O)]^{4-}$ chains and $[Ni(2,2'\text{-bpy})_3]^{2+}$ cations, in which the chain host has a molecular recognition ability for the chiral guest cations. Compound **2** is constructed from linking of the $[As_6V_{15}O_{42}]^{6-}$ polyoxoanions and novel dinuclear $[Zn_2(dien)_3]^{4+}$ cations into the first 1D helical As–V–O cluster chain. Compound **3** is the first 2D framework based on $[As_6V_{15}O_{42}]^{6-}$ polyoxoanions as building blocks.

Introduction

Since the first polyoxometalates (POMs) were reported over 150 years ago, attention has been focused on their synthesis and various structural topologies, as well as their unexpected properties in such diverse fields as catalysis, materials science, and medicine.[1–3] To date, hundreds of POMs based on Mo–O clusters, V–O clusters, and W–O clusters and so on have been synthesized and described.[4,5] They provide a wide variety of robust structural motifs of different sizes and topologies ranging from closed cages and spherical shells to basket-, bowl-, barrel-, and belt-shaped structures. Those intriguing structures and potential applications attract more and more researchers and make the chemistry of POMs of continuous interest.[6] The preparation of extended structure solids with controllable and desirable properties and functions is of both fundamental and practical interest.[7] Now one of the challenging tasks in POM chemistry is to find some bridging units and then to link POM building units up into extended solid frameworks.[8,9] This approach is quite attractive and appears to hold the key to the development of rational approaches for tailor-made materials based on POMs with desirable features. During the past few years, a lot of research efforts have been focused on the application of secondary transition-metal complexes (TMCs) as bridging ligands linking POM clusters into 1-, 2-, and 3D networks under hydrothermal conditions.[10–13] Compounds $[\{Cu(enMe)_2\}_7\{V_{16}O_{38}(H_2O)\}_2]\cdot 4H_2O$[14] and $[Co(en)_2][Co(2,2'\text{-bpy})_2]_2[PMo_8V_8O_{44}]\cdot 4.5H_2O$[15] are recent examples. The former is made up of the hexadecavanadate clusters linked by the $[Cu(enMe)_2]^{2+}$ complex fragments into a rare 3D open framework, while the latter exhibited a novel 2D Mo–V–O polyoxometalate with two types of cobalt complex fragments as bridges. More recently, Khan et al. reported three novel 2D frameworks that consist of spherical $\{V_{18}O_{42}(X)\}$ shells linked by bridging $\{M(en)_2\}$ groups (X = H_2O, Br^-, Cl^-; M = Zn, Cd).[16]

An important subclass of the large POM family is As–V–O clusters with arsenic and vanadium in low oxidation states, which often act as cryptates encapsulating neutral molecules or anions. Since the first As–V–O cluster $K_6[As_6V_{15}O_{42}(H_2O)]\cdot 8H_2O$ was presented by Müller and Döring in 1988,[17] a number of As–V–O clusters have been synthesized,[18–27] such as $K_7[AsV_{14}O_{40}]\cdot 12H_2O$,[18] $Na_5[V_{12}As_8O_{40}(HCO_2)]\cdot 18H_2O$,[19] $[As_8V_{14}O_{42}(X)]^{6-}$ (X = SO_3^{2-} or SO_4^{2-}),[20] $[N(Me)_4]_4[As_8V_{14}O_{42}(0.5H_2O)]$,[21] and $[NBu^n_4]_4[As_8V_6O_{26}]$.[23] However, most of them are discrete clusters; the linking of As–V–O clusters into extended

[a] State Key Laboratory of Structural Chemistry, Fujian Institute of Research on the Structure of Matter, Chinese Academy of Sciences,
Fuzhou, Fujian 350002, China
[b] Department of Applied Chemistry, Faculty of Science, Beijing University of Chemical Technology,
Beijing 100029, China
[c] State Key Laboratory of Inorganic Synthesis and Preparative Chemistry, Jilin University,
Changchun, Jilin 130023, China
[d] State Key Laboratory of Coordination Chemistry, Nanjing University,
Nanjing, Jiangsu 210093, China
Fax: +86-591-8371-0051
E-mail: ygy@ms.fjirsm.ac.cn

Supporting information for this article is available on the WWW under http://www.eurjic.org or from the author.

structures remains largely unexplored and a rewarding challenge. The aim of our work is to synthesize extended solids based on As–V–O clusters in the presence of TMCs. By this means, we recently successfully prepared a novel 2D sinusoidal layer structure constructed from $[As_8V_{14}O_{42}(SO_4)]^{6-}$ clusters and $[Ni(en)_2]^{2+}$ fragments.[28] As a part of continuing work in this system, here we describe the hydrothermal synthesis and structural characterization of the following three extended POMs based on $[As_6V_{15}O_{42}(H_2O)]^{6-}$ clusters as building blocks: $[Ni(2,2'\text{-bpy})_3]_2[\{Ni(en)_2\}As_6V_{15}O_{42}(H_2O)]\cdot 9.5H_2O$ (**1**), a 1D straight chain, $[Zn_2(dien)_3(H_2O)_2]_{1/2}\{[Zn_2(dien)_3]As_6V_{15}O_{42}(H_2O)\}\cdot 2H_2O$ (**2**), a 1D helical chain, and $[Co(enMe)_2]_3[As_6V_{15}O_{42}(H_2O)]\cdot 2H_2O$ (**3**), which is the first 2D $[As_6V_{15}O_{42}(H_2O)]^{6-}$ framework.

Results and Discussion

Compounds **1**–**3** are made of the $[As_6V_{15}O_{42}(H_2O)]^{6-}$ (As_6V_{15}) clusters linked by corresponding TMCs into extended structures. The structure of the As_6V_{15} anion, which has crystallographic D_3 symmetry, was first reported by Müller and Döring in $K_6[As_6V_{15}O_{42}(H_2O)]\cdot 8H_2O$.[17] It consists of fifteen VO_5 square pyramids and three handle-like As_2O_5 units. As shown inpart a of Figure 1, twelve VO_5 square pyramids form two triangles by sharing edges and sharing corners. In addition, another three VO_5 square pyramids and three As_2O_5 units are alternately joined together to form a ring (Figure 1, b). Then the two triangles are coordinated to each face the ring through sharing O

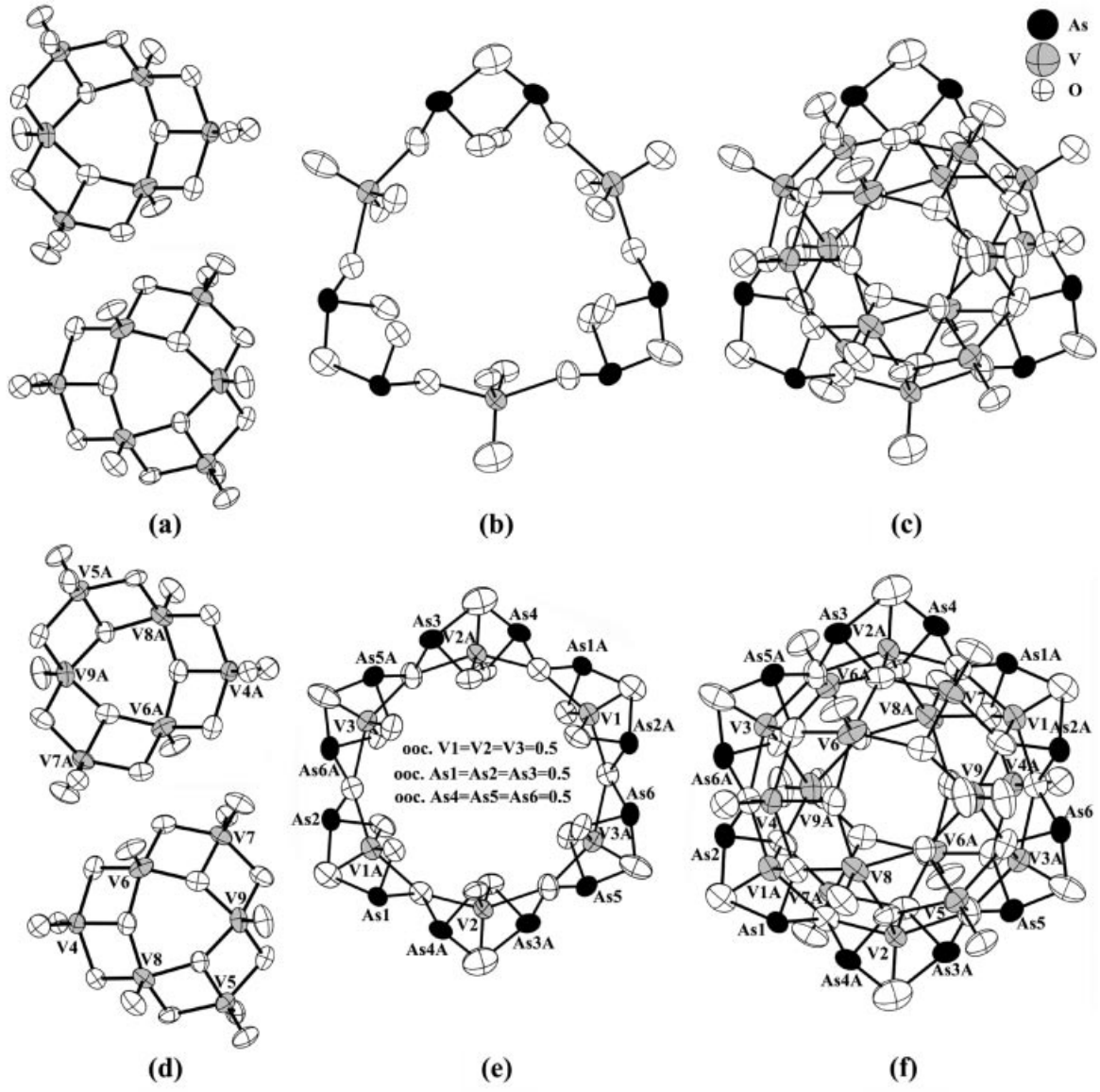

Figure 1. Structural contrast between normal $[As_6V_{15}O_{42}]^{6-}$ anion and disordered $[As_6V_{15}O_{42}]^{6-}$ anion in **1**. (a, b) Two V_3 triangles and one As_6V_3 ring in the normal $[As_6V_{15}O_{42}]^{6-}$ anion, respectively. (c) The normal $[As_6V_{15}O_{42}]^{6-}$ anion. (d, e) Two V_3 triangles and one disordered As_6V_3 ring in the disordered $[As_6V_{15}O_{42}]^{6-}$ anion in **1**. (f) The disordered $[As_6V_{15}O_{42}]^{6-}$ anion in **1**. (The thermal ellipsoids are shown at 50% probability.)

atoms, and form a ball-like As_6V_{15} anion (Figure 1, c). In the structure of the As_6V_{15} cluster in **1**, twelve VO_5 square pyramids form two identical triangles as described above (Figure 1, d). However, an interesting phenomenon is that the ring in the As_6V_{15} anion of **1** was found to be disordered. As shown in Figure 1 (e), three positions occupied by As_2O_5 units are disordered over six positions with free refined occupancy of 0.5 for each position. At the same time, three positions occupied by VO_5 square pyramids are also disordered over six positions (V1, V2, V3, V1A, V2A, and V3A atoms) with free refined occupancy of 0.5 for each position. Then, similarly, the two triangles are coordinated to each face of the disordered ring through sharing O atoms, and form a disordered As_6V_{15} anion (Figure 1, f). The structure of the disordered As_6V_{15} anion in **1** can also be described as a well-known $\{V_{18}O_{42}\}$ rhombicuboctahedron[29] embedded with an arsenic ring (Figure S1). The As_6V_{15} anion in **2** and **3** is essentially identical to that of the isolated cluster in $K_6[As_6V_{15}O_{42}(H_2O)]\cdot 8H_2O$[17] and is not disordered. In **1**–**3**, all V=O, V–O, and As–O bond lengths fall in the ranges 1.520(5)–1.631(6), 1.817(10)–2.107(9), and 1.748(6)–1.887(5) Å, respectively. On the basis of bond valence sum (Σ_s) calculations,[30] the oxidation states of all V atoms are +4 (Σ_s = 4.04–4.48, **1**; Σ_s = 4.02–4.15, **2**; Σ_s = 4.03–4.16, **3**) and the As atoms are +3 (Σ_s = 2.73–2.99, **1**; Σ_s = 3.05–3.20, **2**; Σ_s = 3.04–3.18, **3**). The oxidation states of the V atoms and the As atoms are consistent with the formulas of **1**–**3**. The EPR spectra of **1** and **2** at room temperature show the *g* values are 1.9591 and 1.9493, corresponding to the signal of V^{4+}, respectively. For **3**, no EPR signal of V^{4+} was observed in **3** at room temperature. But at liquid nitrogen temperature, the EPR spectrum of **3** shows the *g* value is 1.9631, corresponding to the signal of V^{4+}.

The extended structure of **1** consists of disordered As_6V_{15} sphere-like clusters. Each one is linked to two other neighboring clusters by two $[Ni2(en)_2]^{2+}$ bridges, generating a 1D straight chain of $[-As_6V_{15}-\mu_2\text{-}Ni2(en)_2-As_6V_{15}-]_\infty$ arrays (Figure 2). The bridging Ni2 atom shows an octahedron with four nitrogen donors of two en ligands [Ni2–N: 2.040(2)–2.061(18) Å] and two *trans* terminal oxo oxygen atoms coming from two adjacent VO_5 groups [Ni2–O: 2.199(11) Å, O–Ni2–O: 180(8)°]. An interesting feature is that another kind of TMC $[Ni1(2,2'\text{-bpy})_3]^{2+}$ rather than $[Ni(en)_3]^{2+}$ occupies the interchain regions as charge compensation. As shown in Figure 3, the $\{[Ni(en)_2]As_6V_{15}O_{42}(H_2O)\}^{4-}$ chains are aligned to the *b* axis and parallel packed beside each other along the *a* axis, generating a cluster anion layer along the *ab* plane, while the $[Ni(2,2'\text{-bpy})_3]^{2+}$ cations are exactly deposited between cluster anion layers

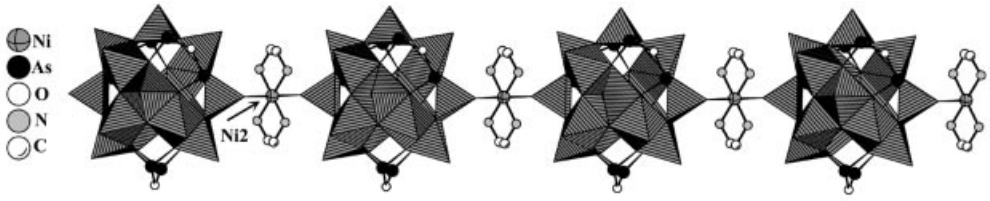

Figure 2. A view of the infinite straight chain in **1**. Half of the disordered atoms and H atoms were omitted for clarity.

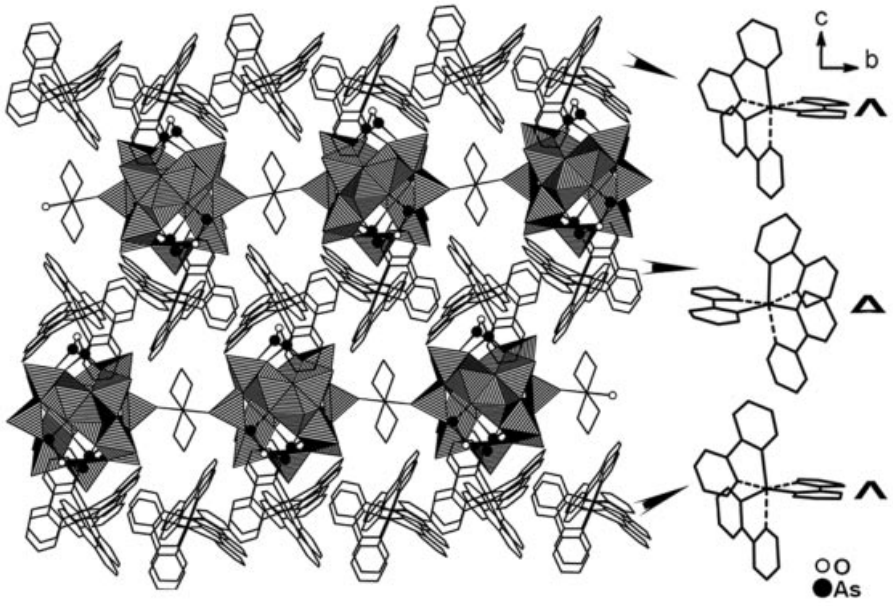

Figure 3. Packing diagrams of **1** along the *a* axis showing host chains have a molecular recognition ability for the guest metal complexes. All H atoms were omitted for clarity.

to form the cation layer along the *ab* plane. The $[Ni(2,2'\text{-bpy})_3]^{2+}$ cations in **1** present both Δ and Λ enantiomers. An unusual feature is that the Δ and Λ enantiomers of $[Ni(2,2'\text{-bpy})_3]^{2+}$ are separated orderly and deposited in alternate cluster anion layer regions, that is, the isolated $[Ni(2,2'\text{-bpy})_3]^{2+}$ cations are separated into Δ configuration layers and Λ configuration layers by cluster chain layers. The orderly separation of the enantiomers of $[Ni(2,2'\text{-bpy})_3]^{2+}$ indicates that the inorganic host has a molecular recognition ability for the guest TMCs.[31] Such a phenomenon is rarely reported in the POM system. The shortest inter-ring separation of 2,2′-bpy ligands along the *a* axis is 12.27 Å, hence, there is no notable π–π interaction in **1**.

POMs with helical or chiral structures are of particular interest.[32] For instance, a spiral-shaped chain has been described in $[H_2en]_2[\{Cu(en)(OH_2)\}Mo_5P_2O_{23}]\cdot 4H_2O$[33] and a double helical chain in $[(CH_3)_2NH_2]K_4[V_{10}O_{10}(H_2O)_2(OH)_4(PO_4)_7]\cdot 4H_2O$.[34] Single-crystal X-ray diffraction analysis revealed that compound **2** presents the first helical chain made of As–V–O clusters. As shown in Figure 4, the As_6V_{15} clusters are connected to each other through novel $[(dien)Zn1(dien)Zn2(dien)]^{4+}$ dimeric cations by corner-sharing interactions of the type V=O–Zn1 to form an infinite 1D chain along the *b* axis, which arranged about a twofold screw axis and formed a left-hand helical array. Because compound **2** crystallizes in a centric space group $P2_1/c$, there are an equal number of right-handed (Figure S2) and left-handed helices (Figure 4) in the structure. As illustrated in Figure 5, it is interesting that the right-handed helical chains and the left-handed helical chains are aligned parallel to the *ab* plane to give right-handed helical chain layers and left-handed helical chain layers, respectively. Furthermore, these right-handed helical chain layers and left-handed helical chain layers are alternatively stacked along the *c* axis with another kind of novel dimeric cation, $[Zn_2(dien)_3(H_2O)_2]^{4+}$, occupying the interlayer regions (Figure 5, Figure 6). Hydrogen bonds play important roles in stabilizing the crystal structure of **2**. The isolated $[Zn_2(dien)_2(H_2O)_5]^{4+}$ cations link the chains through three pairs of hydrogen bonds [N10–O40a (a: $-x$, $y + 1/2$, $-z + 1/2$), 3.01(2) Å; N10–O37b (b: $-x$, $-y + 1$, $-z$), 3.25(3) Å; and N11–O41 3.02(2) Å, respectively] generating 2D networks along the *bc* plane, while $[Zn_2(dien)_3]^{4+}$ bridging cations interact with the chains along the *a* axis through strong hydrogen bonds [N···O: 2.835(10)–3.175(10) Å, listed in Table S1]. These hydrogen bonds force the structure of compound **2** to extend into a 3D supramolecular array.

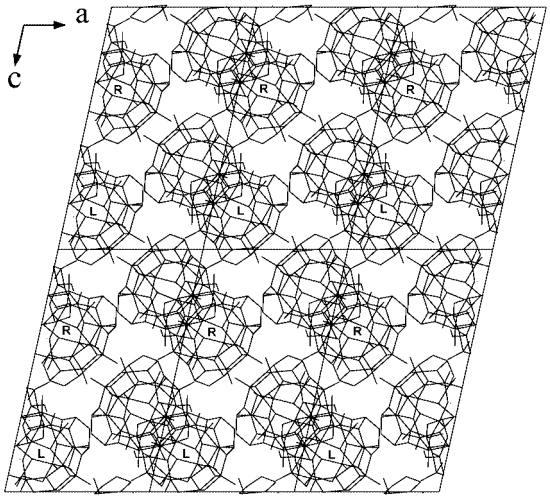

Figure 5. Packing diagram of **2** viewed along the *b* axis showing alternative right-hand and left-hand helical chain layers. All H atoms, water molecules, and isolated $[Zn_2(dien)_3(H_2O)_2]^{4+}$ cations are omitted for clarity.

The second unusual feature of **2** is that each Zn1(dien) bridging fragment hangs a $[Zn2(dien)]^{2+}$ complex linked through a tridentate dien ligand to form a novel dinuclear

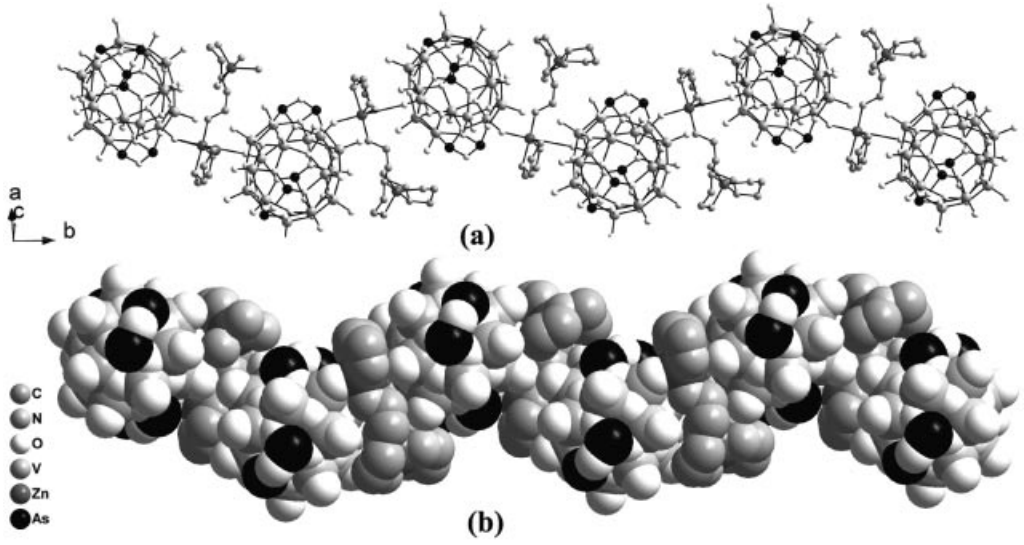

Figure 4. A ball-and-stick (a) and a space-filling (b) view of the left-hand helical chain of **2** showing the connectivity between the $[As_6V_{15}O_{42}(H_2O)]^{6-}$ clusters and $[Zn_2(dien)_3]^{4+}$ complexes and orientation of the chain. (Structure of right-hand helical chain of **2** can be seen in Figure S2.) All H atoms were omitted for clarity.

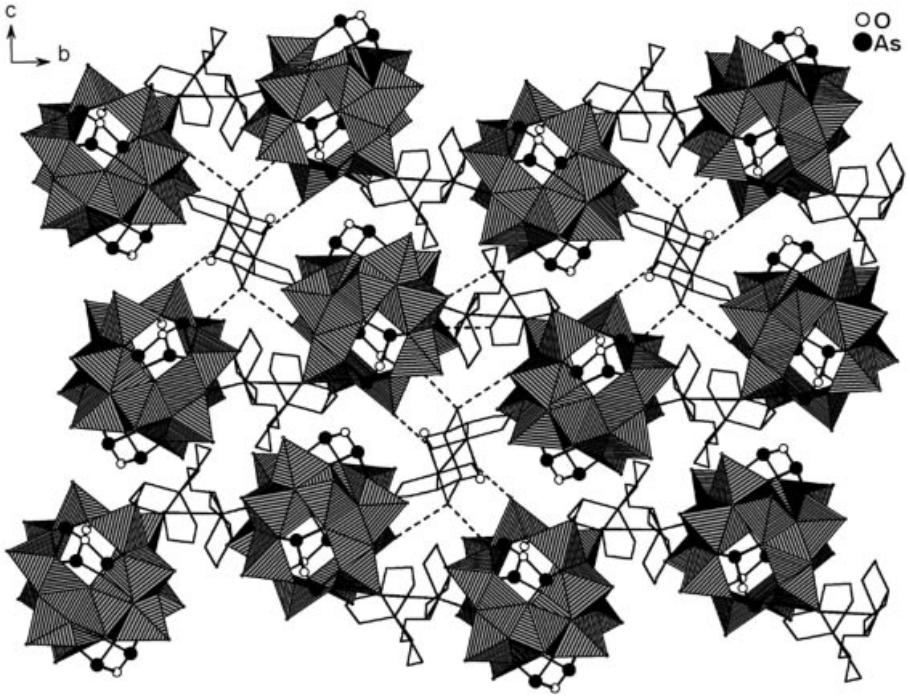

Figure 6. View of the 2D networks of **2** along the *a* axis showing the hydrogen bonds between helical chains and discrete $[Zn_2(dien)_3(H_2O)_2]^{4+}$ cations.

$[(dien)Zn1(dien)Zn2(dien)]^{4+}$ cation (Figure 7, b). Two N atoms of the bridging dien ligand coordinate to the Zn2 center, while the third N atom coordinates to the Zn1 center. Each Zn atom in dinuclear TMC is bound to two dien ligands in different coordination modes, respectively. Thus the Zn1 center is defined by four N donors from two dien ligands and two *trans* terminal oxo oxygen atoms from two adjacent arsenic–vanadium clusters to form a distorted octahedron [Zn1–N: 1.981(7)–2.155(9) Å; Zn1–O: 2.142(5) Å], whereas the five-coordinate Zn2 center is best described as a distorted trigonal bipyramidal configuration, with the atoms N5 and N8 occupying the axial positions [Zn2–N5: 2.265(8) Å; Zn2–N6: 2.049(6) Å; Zn2–N7: 2.081(7) Å; Zn2–N8: 2.187(7) Å; Zn2–N9: 2.017(9) Å]. Khan et al. has recently reported an unexpected binuclear $[Zn_2(en)_5]^{4+}$ cation (Figure 7, a) in compound $[Zn_2(en)_5][\{Zn(en)_2\}_2V_{18}O_{42}(H_2O)]\cdot 9H_2O$.[16] One striking difference between $[Zn_2(dien)_3]^{4+}$ and $[Zn_2(en)_5]^{4+}$ cations is that the former act as μ_2-bridging units that link As_6V_{15} clusters to form a 1D chain, while the latter just act as balance cations. Another distinct difference is that the $[Zn_2(en)_5]^{4+}$ cation is a centrosymmetric ion and the two zinc sites display the same coordination environments: distorted ZnN_5 trigonal bipyramidal configuration, while the $[Zn_2(dien)_3]^{4+}$ cation is a noncentral ion and two independent zinc sites display two kinds of different coordination environments: distorted N_4Zn1O_2 octahedron and distorted $Zn2N_5$ trigonal bipyramid. The average Zn–N distance (2.120 Å) in $[Zn_2(dien)_3]^{4+}$ is somewhat shorter than that of the $[Zn_2(en)_5]^{4+}$ cation (2.134 Å). The Zn1···Zn2 separation distance [6.492(7) Å] in the $[Zn_2(dien)_3]^{4+}$ cation is obviously shorter than that of the $[Zn_2(en)_5]^{4+}$ cation [7.592(2) Å].

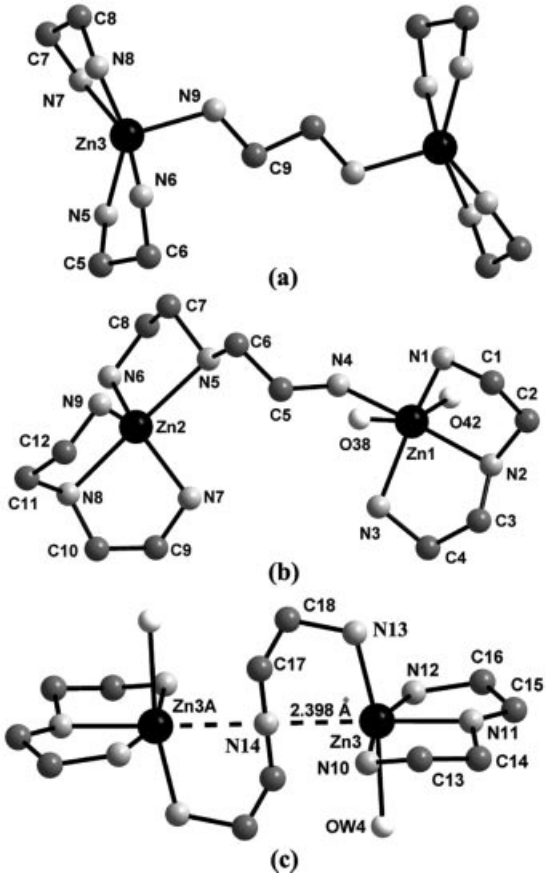

Figure 7. (a) Structure of binuclear TMC in ref.[16]. (b, c) Structures of binuclear TMCs in **2**, showing two unique coordination modes. All the H atoms are omitted for clarity.

The third unusual feature of **2** is that the structure contains another kind of novel isolated binuclear $[Zn_2(dien)_3(H_2O)_2]^{4+}$ cation providing charge compensation (Figure 7, c). The structure of the $[Zn_2(dien)_3(H_2O)_2]^{4+}$ cation can be described as two $[Zn(dien)(H_2O)]^{2+}$ moieties linked across an inversion center by a bridging dien ligand. The two terminal N13 and N13A atoms of bridging dien exhibit strong attachment to the Zn3 and Zn3A atoms, respectively, with Zn–N distances of 2.036(18) Å, while the middle N14 atom occupies the central site of the binuclear cation and exhibits weak attachment to both Zn3 and Zn3A atoms with Zn–N distances of 2.398(3) Å, which are much longer than the usual Zn–N values (about 1.90–2.20 Å) observed in many reported studies.[16,35,36] Such a coordination mode between the Zn atoms and the bridging dien ligand is peculiar. The Zn3–O distance [2.430(2) Å] and the bond valence sum[30] value (0.17) identify the O atom coordinated to the Zn3 center as H_2O (denoted as OW4 in this paper). The Zn3···Zn3A separation distance [4.796(10) Å] is even shorter than that of Zn1···Zn2 [6.493(7) Å].

The solid architectures of **1** and **2** provide examples of a different way of connecting As_6V_{15} clusters and TMCs groups. This suggests that further condensation of As_6V_{15} clusters into higher dimensional solids through the linkage of TMCs groups could be feasible. Suitable modification of the synthetic conditions results in the successful crystallization of solid **3**, which is the first 2D As_6V_{15} framework. As shown in Figure 8, the As_6V_{15} cluster acts as a hexadentate ligand coordinating to six Co^{2+} ions through the terminal oxo oxygen atoms with Co–O distances ranging from 2.180(6) to 2.278(6) Å, such that each As_6V_{15} cluster is connected with six others through *trans*-{$Co(enMe)_2O_2$} groups to generate a 2D framework (Figure 9). Each Co atom in **3** acts as a bridge and is located at a distorted octahedral center, being coordinated by two O atoms from the arsenic–vanadium polyoxoanion and four N atoms from two enMe ligands with Co–N bond lengths ranging from 2.049(8) to 2.110(9) Å. These layers are stacked along the [1$\bar{1}$0] direction in AAAA sequence with an interlamellar separation of approximately 9.0 Å (see Figure S3 in the Supporting Information), forming *pseudo*-1D channels along the *c* axis, which are occupied by lattice water molecules and organic ligands (Figure S4).

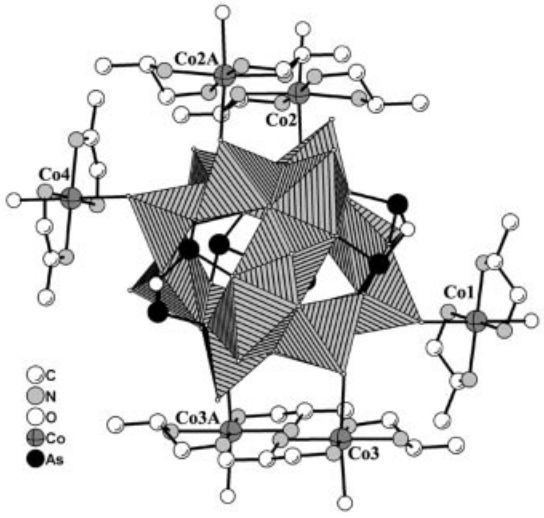

Figure 8. View of coordination mode of the $[As_6V_{15}O_{42}(H_2O)]^{6-}$ cluster in **3**.

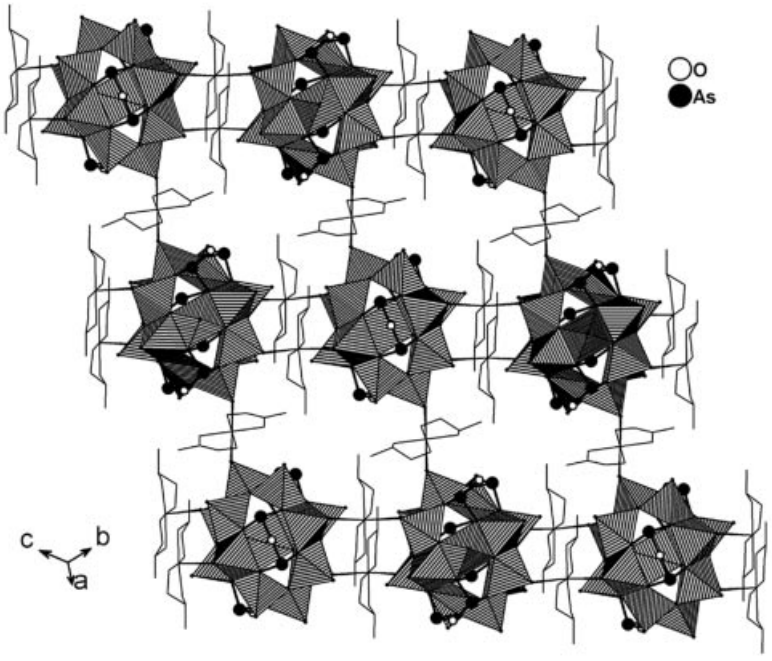

Figure 9. View of the 2D structure of **3** along the [111] direction. All the H atoms and water molecules are omitted for clarity.

The infrared spectrum of **1** exhibited features characteristics of ν(M–O–M) (M = V or As) in the 480–800 cm^{-1} regions. The strong bands at 983 can be assigned to the stretching vibrations of V=O bonds. The region of interest in determining the mode of 2,2′-pyridine binding and the bending bands of the NH_2 and CH_2 are from 1161–1599 cm^{-1}. The infrared spectrum of **2** shows the bending bands of the NH_2 and CH_2 present at around 1583, 1458, and 1362 cm^{-1}. While the strong peak 980 cm^{-1} is attributed to the vibrations of V=O bands, a series of bands in the 480–760 cm^{-1} region is characteristic of ν(M–O–M) (M = V or As) and ν(As–O). The infrared spectrum of **3** exhibits a number of absorption bands in the 1100–1600 cm^{-1} region. Many of these bands are attributed to the fundamental vibration modes of enMe. The strong and sharp bands at 973 cm^{-1} are assigned to the vibrations of V=O bands. Furthermore a broad band between 833 and 500 cm^{-1} with maximum at 701 cm^{-1} is attributed to asymmetric and symmetric {M–O–M} (M = V or As) stretching. These positions of the bands and their assignments of **1**–**3** are consistent with literature reports.[16,24,37]

The thermogravimetric analyses were carried out in flowing N_2 with a heating rate of 10 °C·min^{-1} in the temperature range 30–1000 °C for compounds **1**–**3** (Figure 10). Three distinct weight-loss stages are observed on the TGA curve of compound **1**. The first stage, which occurs from 46 to 109 °C, is attributed to the loss of 10.5 water molecules; the observed weight loss (4.84%) is in agreement with the calculated value (5.71%). The remaining two stages occur between 156 and 847 °C, and are due to the loss of two en molecules and six 2,2′-bpy molecules, and the sublimation of three As_2O_3 molecules; the observed weight loss (49.68%) is consistent with the calculated value (49.89%). Assuming that the residue corresponds to VO_2 and NiO, the observed total weight loss (54.52%) is also in agreement with the calculated value (55.59%). The TG curve of **2** shows two major mass losses in the regions 46–132 °C and 178–776 °C. The first step corresponds to the loss of four water molecules (exp. 2.01%, calcd. 2.75%). The second huge mass loss can be assigned to the loss of 4.5 dien molecules and the sublimation of three As_2O_3 molecules (exp. 41.19%, calcd. 40.41%). Assuming that the residue corresponds to VO_2 and ZnO, the observed total weight loss (43.20%) is in good agreement with the calculated value (43.16%). The TG curve of **3** indicates that the weight loss of **1** cannot be completely divided into distinct stages. The whole stage, which occurs from 58 to 786 °C, is attributed to the loss of H_2O and enMe, and the sublimation of As_2O_3. Assuming that the residue corresponds to VO_2 and CoO, the observed weight loss (43.29%) is in good agreement with the calculated value (42.74%).

The variable temperature magnetic susceptibilities of **1** and **2** were measured between 2 and 300 K. Figure 11 shows the magnetic behaviors of **1** and **2** in the form of the product $\chi_M T$ versus temperature, where χ_M is the molar magnetic susceptibility. The $\chi_M T$ value of complex **1** at 300 K is 3.33 cm^3·mol^{-1}·K, much smaller than the expected value (8.40 cm^3·mol^{-1}·K) for the fifteen uncoupled S = 1/2 spins of V^{4+} atoms (5.40 cm^3·mol^{-1}·K, g = 1.9591 for V^{4+} from EPR result) and three uncoupled S = 1 spins of the Ni^{2+} atoms (3.0 cm^3·mol^{-1}·K, g = 2.0). Upon cooling, the $\chi_M T$ value decreases nearly linearly to 2.48 cm^3·mol^{-1}·K at 50 K, and then decreases rapidly from 50 K and reaches a minimum value of 1.74 cm^3·mol^{-1}·K at 2 K. Such magnetic behavior is characteristic of the combination of zero-field splitting of Ni^{2+} in distorted octahedral environments and strong antiferromagnetic couplings between adjacent paramagnetic centers. The short V···V distance (≤ 3.006 Å) and structural disorder of V^{4+} ions are probably mainly responsible for the strong magnetic interaction at high temperature.[38–40] For **2**, $\chi_M T$ at room temperature is 1.83 cm^3·mol^{-1}·K, which is also much lower than the value expected for 15 uncoupled electrons (5.34 cm^3·mol^{-1}·K, g = 1.9493 for V^{4+} from EPR result). As the temperature decreases, the $\chi_M T$ value decreases rapidly until 150 K to stabilize approximately at 1.08 cm^3·mol^{-1}·K. Below 25 K another faster decrease of $\chi_M T$ is observed, with about 0.47 cm^3·mol^{-1}·K at 2.0 K. Because the Zn^{2+} ion is nonmagnetic, the magnetic behavior of **2** can be attributed to the exchange interactions between V^{4+} ions in $[As_6V_{15}O_{42}]^{6-}$

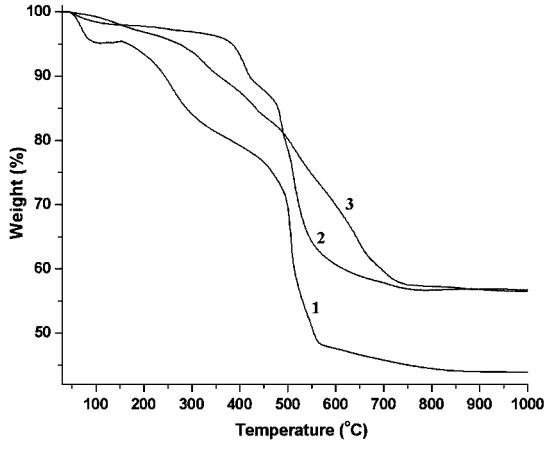

Figure 10. TGA curves of compounds **1**–**3**.

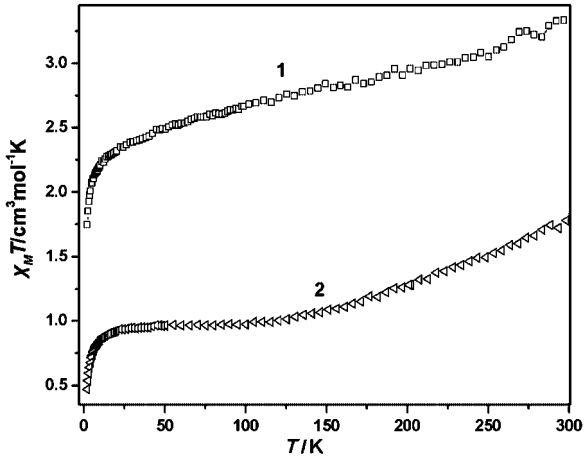

Figure 11. The temperature dependences of the product $\chi_M T$ for **1** and **2**.

polyoxoanions. The short neighboring V···V distances of V1···V3 (2.846 Å), V2···V4 (2.834 Å), V5···V6 (2.839 Å), V10···V11 (2.868 Å), V12···V13 (2.885 Å), and V14···V15 (2.882 Å) pairs with double O bridges lie in the range expected for strong antiferromagnetic coupling,[29,38–40] thus resulting in a low $\chi_M T$ value at high temperature. The remaining three vanadium ions are largely uncorrelated at high temperature. When temperature is lowered further, a weak antiferromagnetic coupling occurs between these three vanadium centers through the $[As_2O_5]^{4-}$ bridge, which corresponds to the second decrease below 25 K. The value (1.08 $cm^3 \cdot mol^{-1} \cdot K$) of the plateau of $\chi_M T$ in the range 150–25 K is in agreement with the calculated value for three uncoupled V^{4+} ions.

The temperature dependences of $\chi_M T$ for **1** and **2** demonstrate the existence of strong antiferromagnetic coupling interactions, which are a common feature for most polyoxovanadate clusters.[29,41] Unfortunately, it is too difficult to fit the experimental magnetic data of these extended high-nuclearity heteropolymetallic spin systems using a suitable theoretical model.[42]

Conclusions

In this paper, we have described three extended As–V–O compounds synthesized by a hydrothermal method, all constructed from $[As_6V_{15}O_{42}(H_2O)]^{6-}$ cluster units. These results emphasize the potential of $[As_6V_{15}O_{42}(H_2O)]^{6-}$ clusters as building blocks for constructing new materials and demonstrate that the hydrothermal techniques are a vital tool for the realization of materials design. Moreover, the construction of these new materials may facilitate the formation of unexpected species[16] such as the novel $[Zn_2(dien)_3]^{4+}$ and $[Zn_2(dien)_3(H_2O)_2]^{4+}$ cations observed during the course of this work. Linking discrete POMs to build solid-state materials is of great interest not only from a structural point of view, but also because they are potentially interesting for applications in different areas. Further research will concentrate on the suitable modification of the synthetic conditions to obtain 3D As–V–O cluster architecture, which has never been reported to date to the best of our knowledge and is a challenging task.

Experimental Section

General Remarks: All reagents were purchased commercially and used without further purification. The contents of V, Ni, Zn, Co, and As were determined with an Utlima2 spectrometer. Elemental analyses (C, H, and N) were performed on an Elementar Vario III analyzer. IR spectra were recorded with an ABB Bomem MB102 spectrometer in KBr pellet. Thermal analyses were performed in a dynamic nitrogen atmosphere with a heating rate of 10 °C·min^{-1}, using a METTLER TGA/ SDTA851^e thermal analyzer. EPR spectra were carried out on powder samples at X-band frequency with a Bruker ER-420 spectrometer at room temperature. Variable temperature susceptibility measurements were carried out in the temperature range 2–300 K at a magnetic field of 1 T on polycrystalline samples with a SQUID MPMS-7 magnetometer manufactured by Quantum Design. Background corrections for the sample holder assembly and diamagnetic components of the compound were applied.

Synthesis of $[Ni(2,2'\text{-bpy})_3]_2[\{Ni(en)_2\}As_6V_{15}O_{42}(H_2O)]\cdot 9.5H_2O$ (1): A mixture of V_2O_5 (0.30 g, 1.65 mmol), As_2O_3 (0.10 g, 0.51 mmol), $Ni(CH_3COO)_2\cdot 4H_2O$ (0.05 g, 0.20 mmol), 2,2′-bpy (0.05 g, 0.32 mmol), en (0.30 mL), and H_2O (12 mL, 0.67 mol) was heated to 160 °C for 3 days and then cooled to room temperature. The product was isolated as brown blocks (0.473 g, 65.1% yield based on V). $C_{64}H_{85}As_6N_{16}Ni_3O_{52.50}V_{15}$ (3308.23): calcd. C 23.21, H 2.59, As 13.59, N 6.77, Ni 5.32, V 23.10; found C 22.96, H 2.71, As 13.16, N 6.58, Ni 5.09, V 22.94. IR (KBr) for **1**: $\tilde{\nu}$ = 1632 (m), 1599 (s), 1491 (w), 1471 (m), 1442 (s), 1318 (m), 1161 (w), 1020 (m), 983 (s), 778 (s), 754 (s), 738 (s), 633 (m), 488 (w), 464 (m) cm^{-1}.

Synthesis of $[Zn_2(dien)_3(H_2O)_2]_{1/2}[\{Zn_2(dien)_3\}As_6V_{15}O_{42}(H_2O)]\cdot 2H_2O$ (2): A mixture of V_2O_5 (0.20 g, 1.10 mmol), As_2O_3 (0.24 g, 1.21 mmol), dien (0.40 mL), $Zn(CH_3COO)_2\cdot 2H_2O$ (0.54 g, 2.10 mmol), and H_2O (15 mL, 0.83 mol) was sealed in a Teflon-lined steel autoclave and heated to 160 °C for 3 days and then cooled to room temperature. The product was isolated as brown blocks (0.220 g, 57.3% yield based on V). $C_{18}H_{66.5}As_6N_{13.5}O_{46}V_{15}Zn_3$ (2618.08): calcd. C 8.25, H 2.56, As 17.17, N 7.22, V 29.19, Zn 7.49; found C 7.64, H 2.63, As 16.75, N 6.77, V 30.16, Zn 7.06. IR (KBr) for **2**: $\tilde{\nu}$ = 1583 (s), 1458 (m), 1386 (w), 1362 (w), 1326 (w), 1285 (w), 1144 (m), 1092 (m), 980 (s), 738 (s), 633 (s), 541 (m), 484 (m), 460 (m) cm^{-1}.

Synthesis of $[Co(enMe)_2]_3[As_6V_{15}O_{42}(H_2O)]\cdot 2H_2O$ (3): A mixture of V_2O_5 (0.55 g, 3.02 mmol), As_2O_3 (0.20 g, 1.01 mmol), $H_2C_2O_4\cdot 2H_2O$ (0.382 g, 3.04 mmol), enMe (0.30 mL), $CoSO_4\cdot 4H_2O$ (0.34 g, 1.50 mmol), and H_2O (10 mL, 0.55 mol) was sealed in a Teflon-lined steel autoclave and heated to 160 °C for 6 days and then cooled to room temperature. The product was isolated as brown blocks (0.282 g, 27.3% yield based on V). $C_{18}H_{72}As_6Co_3N_{12}O_{45}V_{15}$ (2567.29): calcd. C 8.44, H 2.83, As 17.51, Co 6.89, N 6.55, V 29.76; found C 8.25, H 2.96, As 16.92, Co 6.80, N 6.38, V 29.05. IR (KBr) for **3**: $\tilde{\nu}$ = 1633 (m), 1578 (s), 1448 (m), 1300 (w), 1267 (m), 1081 (m), 1020 (s), 973 (s), 701 (s), 510 (s), 446 (m) cm^{-1}.

X-ray Crystallography: Crystal structure determinations by X-ray diffraction were performed with a Siemens SMART CCD diffractometer with graphite-monochromated Mo-K_α (λ = 0.71073 Å) radiation in the ω scanning mode at room temperature. The program SADABS was used for the absorption correction. The structures were solved by the direct methods and refined by full-matrix least-squares on F^2. All calculations were performed using the SHELX97 program package. For **1**, in the cluster structure, three positions occupied by As_2O_5 dimers and three positions occupied by VO_5 square pyramids were disordered. Each of the six disordered positions was occupied either by an As_2O_5 dimer or a VO_5 square pyramid. The ratios $[As_2O_5]/[VO_5]$ were refined to 0.5:0.5 for all six disordered positions. The respective occupancies of those disordered As and V atoms were fixed finally according to the value of free refined occupancies. Although the final residuals (R_1 = 0.1122, wR_2 = 0.1967) were relatively large, the molecular anion and transition-metal complexes were well behaved, and there were no unusual temperature factors or excursions of electron density in these regions of the structure. The space group was unambiguous. For **2**, the Zn1 atom was disordered over two positions (Zn1 with SOF = 0.60 and Zn1A with SOF = 0.40). In addition, difference Fourier maps showed two significant regions (7.95 and 2.70 e·Å^{-3}) of electron density close to the Zn3 atom. A disordering effect of the Zn3 atom over three adjacent positions with occupancy of 0.57, 0.38, and 0.05 was therefore modeled. In each structure, hydrogen

Table 1. Crystallographic data for compounds **1**–**3**.

Compound	**1**	**2**	**3**
Formula	$C_{64}H_{85}As_6N_{16}Ni_3O_{52.5}V_{15}$	$C_{18}H_{66.5}As_6N_{13.5}O_{46}V_{15}Zn_3$	$C_{18}H_{72}As_6Co_3N_{12}O_{45}V_{15}$
M_r	3308.23	2618.08	2567.29
Crystal system	monoclinic	monoclinic	triclinic
Space group	$P2_1/n$	$P2_1/c$	$P\bar{1}$
Crystal size [mm]	$0.38\times0.22\times0.22$	$0.20\times0.20\times0.20$	$0.32\times0.40\times0.44$
a [Å]	14.0324(9)	13.361(5)	13.2976(14)
b [Å]	13.9900(8)	23.979(8)	15.0583(12)
c [Å]	30.5785(19)	22.873(8)	20.1661(17)
α [°]	90	90	85.620(8)
β [°]	102.861(1)	102.459(4)	79.553(9)
γ [°]	90	90	65.087(9)
V [Å^3]	5852.4(6)	7155.7(4)	3601.6(6)
Z	2	4	2
D_{calcd} [g·cm^{-3}]	1.877	2.430	2.367
μ [mm^{-1}]	3.378	5.697	5.348
Reflections collected	16866	43070	18415
Unique data (R_{int})	9624(0.0741)	12225(0.0437)	16313(0.0432)
F(000)	3256	5080	2496
θ range [°]	2.00–25.08	2.49–25.03	1.71–27.50
Goodness of fit	1.087	1.075	0.992
R_1, wR_2 [$I > 2\sigma(I)$][a]	0.1122, 0.1967	0.0580, 0.1434	0.0649, 0.1279
$\Delta\rho_{max}$, $\Delta\rho_{min}$ [e·Å^{-3}]	1.622, –1.848	1.784, –1.343	1.767, –1.204

[a] $R_1 = \Sigma||F_o| - |F_c||/\Sigma|F_o|$; $wR_2 = \{\Sigma[w(F_o^2 - F_c^2)^2]/\Sigma[w(F_o^2)^2]\}^{1/2}$.

atoms of organic ligands were geometrically placed and refined using a riding model. These above-mentioned disordered atoms and several disordered C atoms (C31 and C32 in **1**, C6, C7, and C9 in **2**, and C12 in **3**) were refined isotropically; the other atoms were refined anisotropically. Experimental details for the structural determinations of **1**–**3** are presented in Table 1. Ranges of selected bond lengths of **1**–**3** are listed in Table 2.

Table 2. Ranges of some important bond lengths [Å] for compounds **1**–**3**.[a]

1			
V=O_t	1.520(5)–1.624(11)	Ni1–N	2.039(17)–2.110(15)
V–O_b	1.817(10)–2.107(9)	Ni2–N	2.040(2)–2.061(18)
As–O	1.767(5)–1.887(5)	Ni2–O	2.199(11)
2			
V=O_t	1.600(5)–1.623(5)	Zn2–N	2.017(9)–2.265(8)
V–O_b	1.913(4)–2.045(6)	Zn3–N	2.021(16)–2.398(3)
As–O	1.748(6)–1.811(6)	Zn1–O	2.142(5)
Zn1–N	1.981(7)–2.155(9)	Zn3–O	2.430(2)
3			
V=O_t	1.590(6)–1.631(6)	Co4–N	2.095(11)–2.102(11)
V–O_b	1.887(6)–2.042(7)	Co1–O	2.180(6)
As–O	1.750(6)–1.797(6)	Co2–O	2.257(6)–2.278(6)
Co1–N	2.097(8)–2.099(8)	Co3–O	2.221(6)–2.263(6)
Co2–N	2.049(8)–2.080(8)	Co4–O	2.273(7)
Co3–N	2.055(9)–2.110(9)		

[a] O_t, terminal oxygen atoms; O_b, oxygen atoms in basal plane of VO_5 pyramids.

CCDC-254404 (for **1**), -254405 (for **2**), and -259395 (for **3**) contain the supplementary crystallographic data for this paper. These data can be obtained free of charge from The Cambridge Crystallographic Data Centre via www.ccdc.cam.ac.uk/data_request/cif.

Supporting Information: Two Tables of hydrogen bonds of compounds **2** and **3**, and four additional plots for compounds **1**–**3**. This material is available free of charge via the Internet at http://www.eurjic.org or from the authors.

Acknowledgments

This work was supported by the NNSF of China (Nos. 20271050/20473093), the Talents Program of Chinese Academy of Sciences, and the NSF of Fujian Province (Nos. E0510030/E0210029).

[1] D. E. Katsoulis, *Chem. Rev.* **1998**, *98*, 359–388.
[2] M. T. Pope, A. Müller, *Angew. Chem.* **1991**, *103*, 56–70; *Angew. Chem. Int. Ed. Engl.* **1991**, *30*, 34–48.
[3] A. Müller, F. Peters, M. T. Pope, D. Gatteschi, *Chem. Rev.* **1998**, *98*, 239–272.
[4] a) *Gmelin Handbuch der Anorganischen Chemie*, Verlag Chemie, Berlin, System No. 53 (Molybdän), **1935**; System No. 54 (Wolfram), **1933**; b) H. T. Evans Jr, *Perspect. Struct. Chem.* **1971**, *4*, 1–59; c) M. T. Pope, *Heteropoly and Isopoly Oxometalates*, Springer, Berlin, **1983**.
[5] a) V. W. Day, W. G. Klemperer, O. M. Yagi, *J. Am. Chem. Soc.* **1989**, *111*, 5959–5961; b) W. G. Klemperer, T. A. Marquart, O. M. Yagi, *Angew. Chem.* **1992**, *104*, 51–53; *Angew. Chem. Int. Ed. Engl.* **1992**, *31*, 49–51; c) G. K. Johnson, E. O. Schlemper, *J. Am. Chem. Soc.* **1978**, *100*, 3645–3646; d) M. I. Khan, J. Zubieta, *Angew. Chem.* **1994**, *106*, 784–786; *Angew. Chem. Int. Ed. Engl.* **1994**, *33*, 760–762; e) G. Huan, A. J. Jacobson, V. W. Day, *Angew. Chem.* **1991**, *103*, 426–427; *Angew. Chem. Int. Ed. Engl.* **1991**, *30*, 422–423.
[6] a) M. Piepenbrink, M. U. Triller, N. H. J. Gorman, B. Krebs, *Angew. Chem.* **2002**, *114*, 2633–2635; *Angew. Chem. Int. Ed.* **2002**, *41*, 2523–2525; b) M. I. Khan, S. Tabussum, R. J. Doedens, V. O. Golub, C. J. O'Connor, *Inorg. Chem.* **2004**, *43*, 5850–5859; c) K. Hegetschweiler, B. Morgenstern, J. Zubieta, P. J. Hagrman, N. Lima, R. Sessoli, F. Totti, *Angew. Chem.* **2004**, *116*, 3518–3521; *Angew. Chem. Int. Ed.* **2004**, *43*, 3436–3439; d) T. Whitfield, X. Wang, A. J. Jacobson, *Inorg. Chem.* **2003**, *42*, 3728–3733; e) X. M. Zhang, H. S. Hu, F. Q. Zhang, A. Prikhod′ko, S. Kuwata, P. Comba, *Chem. Commun.* **2004**, 2046–2047.
[7] E. Coronado, C. J. Gomez-Garcia, *Chem. Rev.* **1998**, *98*, 273–296.
[8] C. D. Wu, C. Z. Lu, H. H. Zhuang, J. S. Huang, *J. Am. Chem. Soc.* **2002**, *124*, 3836–3837.

[9] D. L. Long, H. Abbas, P. Kögerler, L. Cronin, *J. Am. Chem. Soc.* **2004**, *126*, 13880–13881.
[10] P. J. Hagrman, D. Hagrman, J. Zubieta, *Angew. Chem.* **1999**, *111*, 2798–2848; *Angew. Chem. Int. Ed.* **1999**, *38*, 2638–2684.
[11] J. Lu, E. H. Shen, M. Yuan, Y. G. Li, E. B. Wang, C. W. Hu, L. Xu, J. Peng, *Inorg. Chem.* **2003**, *42*, 6956–6958.
[12] J. R. D. DeBord, R. C. Haushalter, L. M. Meyer, D. J. Rose, P. J. Zapf, J. Zubieta, *Inorg. Chim. Acta* **1997**, *256*, 165–168.
[13] a) M. I. Khan, E. Yohannes, R. J. Doedens, *Angew. Chem.* **1999**, *111*, 1374–1376; *Angew. Chem. Int. Ed.* **1999**, *38*, 1292–1294; b) M. I. Khan, E. Yohannes, D. Powell, *Chem. Commun.* **1999**, 23–24.
[14] C. M. Liu, D. Q. Zhang, M. Xiong, D. B. Zhu, *Chem. Commun.* **2002**, 1416–1417.
[15] B. Z. Liu, S. X. Liu, *Chem. Commun.* **2002**, 2126–2127.
[16] M. I. Khan, E. Yohannes, R. J. Doedens, *Inorg. Chem.* **2003**, *42*, 3125–3129.
[17] A. Müller, J. Döring, *Angew. Chem.* **1988**, *100*, 1789–1789; *Angew. Chem. Int. Ed. Engl.* **1988**, *27*, 1721–1721.
[18] A. Müller, J. Döring, M. I. Khan, V. Wittneben, *Angew. Chem.* **1991**, *103*, 203–205; *Angew. Chem. Int. Ed. Engl.* **1991**, *30*, 210–212.
[19] A. Müller, J. Döring, H. Bögge, *J. Chem. Soc., Chem. Commun.* **1991**, 273–274.
[20] A. Müller, J. Döring, *Z. Anorg. Allg. Chem.* **1991**, *595*, 251–274.
[21] G. Huan, M. A. Greaney, A. J. Jacobson, *J. Chem. Soc., Chem. Commun.* **1991**, 260–261.
[22] G. Q. Huang, S. W. Zhang, Y. G. Wei, M. C. Shao, *Polyhedron* **1993**, *12*, 1483–1485.
[23] E. Dumas, C. Livage, S. Halut, G. Hervé, *Chem. Commun.* **1996**, 243–244.
[24] W.-M. Bu, G.-Y. Yang, L. Ye, J.-Q. Xu, Y.-G. Fan, *Chem. Lett.* **2000**, 462–463.
[25] J. Salta, Y. D. Chang, J. Zubieta, *J. Chem. Soc., Chem. Commun.* **1994**, 1039–1040.
[26] S.-T. Zheng, J. Zhang, G.-Y. Yang, *Eur. J. Inorg. Chem.* **2004**, 2004–2007.
[27] S.-T. Zheng, J. Zhang, G.-Y. Yang, *Inorg. Chem.* **2005**, *44*, 2426–2430.
[28] X.-B. Cui, J.-Q. Xu, Y. Li, Y.-H. Sun, G.-Y. Yang, *Eur. J. Inorg. Chem.* **2004**, 1051–1055.
[29] A. Müller, R. Sessoli, E. Krickemeyer, H. Bögge, J. Meyer, D. Gatteschi, L. Pardi, J. Westphal, K. Hovemeier, R. Rohlfing, J. Döring, F. Hellweg, C. Beugholt, M. Schmidtmann, *Inorg. Chem.* **1997**, *36*, 5239–5250.
[30] I. D. Brown, D. Altermatt, *Acta Crystallogr., Sect. B: Struct. Sci.* **1985**, *41*, 244–247.
[31] Y. Wang, J. Yu, Z. Shi, R. Xu, *Chem. Eur. J.* **2003**, *9*, 5048–5055.
[32] Z. Shi, S. H. Feng, S. Gao, L. R. Zhang, G.-Y. Yang, J. Hua, *Angew. Chem.* **2000**, *112*, 2415–2417; *Angew. Chem. Int. Ed.* **2000**, *39*, 2325–2327.
[33] J. J. Lu, Y. Xu, N. K. Goh, L. S. Chia, *Chem. Commun.* **1998**, 2733–2734.
[34] V. Soghomonian, Q. Chen, R. C. Haushalter, J. Zubieta, C. J. O'Connor, *Science* **1993**, *259*, 1596–1599.
[35] C. Lei, J. G. Mao, Y. Q. Sun, J. L. Song, *Inorg. Chem.* **2004**, *43*, 1964–1968.
[36] S. Natarajan, *Inorg. Chim. Acta* **2003**, *348*, 233–236.
[37] L. J. Zhang, X. L. Zhao, J. Q. Xu, T. G. Wang, *J. Chem. Soc., Dalton Trans.* **2002**, 3275–3276.
[38] T. Yamase, M. Suzuki, K. Ohtaka, *J. Chem. Soc., Dalton Trans.* **1997**, 2463–2472.
[39] D. Gatteschi, B. Tsukerblatt, A. L. Barra, L. C. Brunel, A. Müller, J. Döring, *Inorg. Chem.* **1993**, *32*, 2144–2147.
[40] A. L. Barra, D. Gatteschi, L. Pardi, A. Müller, J. Döring, *J. Am. Chem. Soc.* **1992**, *114*, 8509–8514.
[41] A. Müller, F. Peters, M. T. Pope, D. Gatteschi, *Chem. Rev.* **1998**, *98*, 239–271.
[42] O. Kahn, *Molecular Magnetism*, VCH, Weinheim, Germany, **1993**.

Received: July 29, 2005
Published Online: December 9, 2005

